RESEARCH ARTICLE

Investigation of Post-seismic and Inter-seismic Displacement Field Following 2003 Bam Earthquake in Iran Based on PS-InSAR Technique

Samane Shokrzade[1] · Behzad Voosoghi[1] · Masoome Amighpey[1] · Mostafa Rahmani[1]

Abstract In this paper, Bam post-seismic deformations during 7 years after earthquake have been extracted using persistent scatterer interferometry technique. The results illustrate that the maximum amount of uplift and subsidence displacements along line of sight direction during 2004–2010 after the earthquake are 4.5 ± 0.5 and -4.3 ± 0.5 cm, respectively. The results of displacement field indicate that an exponential function with the relaxation time of 2.5 years can be fitted to the corresponding process. The estimated inter-seismic slip value by the inversion of SAR line-of-sight data after relaxation time is 6.35 ± 0.05 mm. Mechanical time dependent processes in the post-seismic relaxation typically rely on models of poroelastic rebound, afterslip fault dilatancy recovery and viscoelastic relaxation to explain surface displacements field. The time series are inverted for the afterslip distribution on an extension of the co-seismic rupture. The estimated post-seismic slip value is 20.45 ± 0.38 cm. Most of the post-seismic displacement field can be explained in terms of fault slip. The results of post-seismic motion modeling indicate that the poroelastic rebound can be detected using the line-of-sight data and the effect of viscoelastic relaxation in post-seismic displacement is negligible.

Introduction

An earthquake with the magnitude of 6.6 on 26 M_W both amplitude and phase rocked Bam, Iran on 26 December 2003. ENVISAT radar data indicates that the earthquake main shock didn't occur on previously mapped Bam fault, but on an unknown blind strike slip fault extending ~ 12 km southward from the center of the city (Talebian and Fielding 2004; Funning et al. 2005). The capability of interferometry synthetic aperture radar (InSAR) for precise deformation analysis has been shown in various case studies (Gabriel et al. 1989; Amighpey et al. 2014). To extract a source mechanism from earth surface observation, we measured the post-seismic displacement field of earthquake using InSAR. Persistent scatterer (PS) InSAR, technique addresses both the decorrelation and atmospheric problems of conventional small baseline approach. This technique is useful when we have temporal decorrelation and low deformation rate. Moreover this technique can reduce the topography and atmospheric phase. Due to the low rate of post-seismic displacements, this technique is adequately efficient for measuring the earth surface displacement field.

Post-seismic deformation following large earthquakes are considered to be caused by four models: (1) poroelastic rebound due to pore fluid flow in response to main shock induced pore pressure changes (Peltzer et al. 1998) (2) afterslip (fault creep) on or adjacent the co-seismic rupture

✉ Samane Shokrzade
samaneshokrzade@yahoo.com

Behzad Voosoghi
vosoghi@kntu.ac.ir

Masoome Amighpey
amighpey@dena.kntu.ac.ir; amighpey@yahoo.com

Mostafa Rahmani
mostafa_rahmani2@yahoo.com

[1] Faculty of Geodesy and Geomatics Engineering, K. N. Toosi University of Technology (KNTU), Vali_asr St., Mirdamad Conjunction, Tehran, Iran

plane (Barbot et al. 2008) (3) viscoelastic stress relaxation in the lower crust and upper mantle described by standard linear solid (SLS) and Maxwell rheology (Wang et al. 2009; Ryder et al. 2007) (4) dilatancy recovery (Massonnet et al. 1996; Scholz 1974; Fielding et al. 2009). Post-seismic displacement field follows exponential or logarithmic decay laws, which can be observed by InSAR data. Poroelastic rebound occurs in a short time period of months and in near-fault field (Peltzer et al. 1998), whereas after-slip and, mostly, viscoelastic relaxation occurs in a large time interval (Wang et al. 2009). Ryder et al. (2007) showed that post-seismic deformation for 4 years following the 1997 Manyi earthquake can be explained by afterslip and viscoelastic relaxation. Scholz (1974) showed that a broad regional subsidence in earthquake zone is due to recovery of dilatancy. The results are interpreted such that a negative LOS motion over the Bam fault zone is mostly due to dilatancy recovery (Fielding et al. 2009). Surface deformation measurements provide our primary means for recording post-seismic processes such as after-slip, viscoelastic and poroelastic rebound (Barbot and Fialko 2010).

Fielding measured post-seismic deformation for ~3.5 years after the 2003 Bam, Iran, earthquake using a modified small baseline subset algorithm. He removed any long-wavelength deformation signal for reduce long-wavelength errors due to atmospheric effects and imprecise orbit knowledge, so they couldn't resolve post-seismic deformation due to viscoelastic relaxation or afterslip (Fielding et al. 2009). In this paper, post-seismic and inter-seismic deformations have been measured during 7 years after the 2003 Bam earthquake and post-seismic behavior has been separated from the inter-seismic surface displacement. Post-seismic displacement rate is smaller than the co-seismic deformation. Deformations time series have been extracted using persistent scatterer interferometry (PSI) technique that reduces the topography and atmospheric phase. So viscoelastic relaxation and afterslip can be detected using the line-of-sight data.

Earth Surface Deformation Field After Bam Zone Earthquake Measured by PSI

Post-seismic and inter-seismic deformation time series after the 2003 Bam earthquake have been extracted using persistent scatterer interferometry technique. This technique is useful when we have low deformation rate. Because of low rate for post-seismic displacements of Bam, this technique is very useful for measuring the earth surface deformations. This technique can reduce the topography and atmospheric phase (Hooper 2012). In

this paper post-seismic interferograms were constructed, using standard method for persistent scatterers (StaMPS) software.

Persistent Scatterer Interferometry Technique: Application of StaMPS

The StaMPS method uses both amplitude and phase analysis to determine PS probability for individual pixels. Express the phase in xth pixel in the ith interferogram as:

$$\phi_{int,x,i} = \phi_{def,x,i} + \phi_{atm,x,i} + \phi_{orb,x,i} + \phi_{\varepsilon,x,i} + \phi_{n,x,i} \quad (1)$$

where $\phi_{def,x,i}$ is the phase change due to surface deformation, $\phi_{atm,x,i}$ is the phase due to atmosphere delay, $\phi_{orb,x,i}$ is the residual phase due to orbit inaccuracies, $\phi_{\varepsilon,x,i}$ is the residual topographic phase due to error in the DEM and $\phi_{n,x,i}$ is the noise term.

Ferretti et al. (2000) identified PS candidate using the amplitude dispersion index D_A, defines as:

$$D_A \cong \frac{\sigma_A}{\mu_A} \quad (2)$$

where σ_A and μ_A are standard deviation and mean of the series of amplitude values respectively. With selection of a proper threshold value of D_A, number of PS value increases. Hooper (2006) adopted a threshold value $D_A = 0.4$. That is, any pixel with $D_A < 0.4$ is considered PS candidate. Then refined PS probability using phase analysis in an iterative process. Hooper (2006) defined the measure of variation of the residual phase for a pixel as:

$$\gamma_X = \frac{1}{N} \left| \sum_{i=1}^{N} \exp j \left\{ \left(\phi_{int,x,i} - \bar{\phi}_{int,x,i} - \Delta\hat{\phi}_{\varepsilon,x,i} \right) \right\} \right| \quad (3)$$

where N is the number of interferograms, $\bar{\phi}_{int,x,i}$ is the estimate of the wrapped the spatially correlated phase of each of terms on the right side of Eq. (1) and $\Delta\hat{\phi}_{\varepsilon,x,i}$ is the spatially uncorrelated part of $\Delta\phi_{\varepsilon,x,i}$. After each iteration the root-mean-square change in coherence γ_X, is calculated. When the solution is converged, the algorithm stops iterating.

Deformation Field of After Bam Earthquake

Details of the radar data used in this study are illustrated in Table 1. From this acquisition, 11 post-seismic interferograms were constructed, using StaMPS software. The image 2005/12/07 that minimizes the sum decorrelation of all the interfrograms been selected for master image. Post-seismic time series after Bam, Iran earthquake in far-fault field (Jackson 2006) is shown in Fig. 1.

To remove topographic effects from the interfrogram 3 arc SRTM DEM was applied (Fig. 2). Because the ~7 m

Table 1 Details of ENVISAT images used in this study

Orbit	Date YYYYMMDD	Perpendicular baseline $B\perp$ (m)	Temporal baseline (day)
10194	20040211	70.7	−665
11169	20040421	352.4	−595
14202	20041117	−186.2	−385
15204	20050126	59.2	−315
18711	20050925	92.4	−70
31971	20051207	0	0
21216	20060322	238.3	105
24222	20061018	−265.9	315
28230	20070725	24.3	595
32238	20080430	−80.7	875
37749	20090520	−35.9	1260
44262	20100818	−22.4	1715
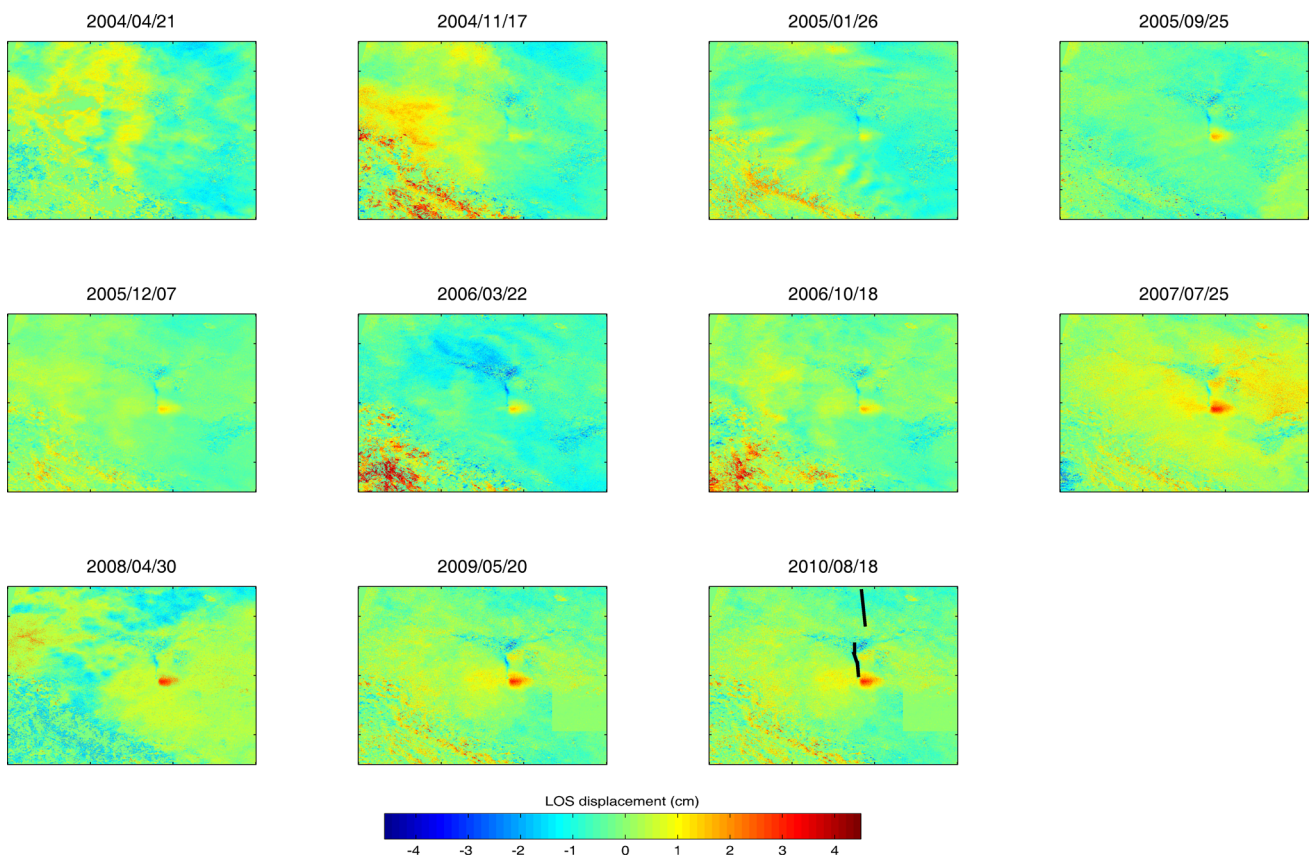
Fig. 1 Postseismic time series after Bam, Iran earthquake in far-fault field. *Black Lines* in *bottom image* marks location of Bam faults

vertical uncertainty in SRTM data (Funning et al. 2005), the topography phase was not removed completely from southwest of the interfrograms with dates 2004/04/21, 2006/10/18, 2006/03/22,2004/11/17 that have greater baselines.

Because poroelastic rebound and afterslip occurs in near fault location, so for studying Post-seismic deformation, time series in near-fault field is shown in Fig. 3.

In the post-seismic displacement field is a lobe of positive line of sight motion (towards the satellite locations) to the southeast of the rupture (feature A on Fig. 4). The post-seismic InSAR shows that there is a negative LOS motion over the Bam fault zone (feature B on Fig. 4).

The precision of displacement field is important. The standard deviation of the estimated displacement field is shown in Fig. 5.

Fig. 2 DEM produced from
SRTM was used to remove
topographic fringes
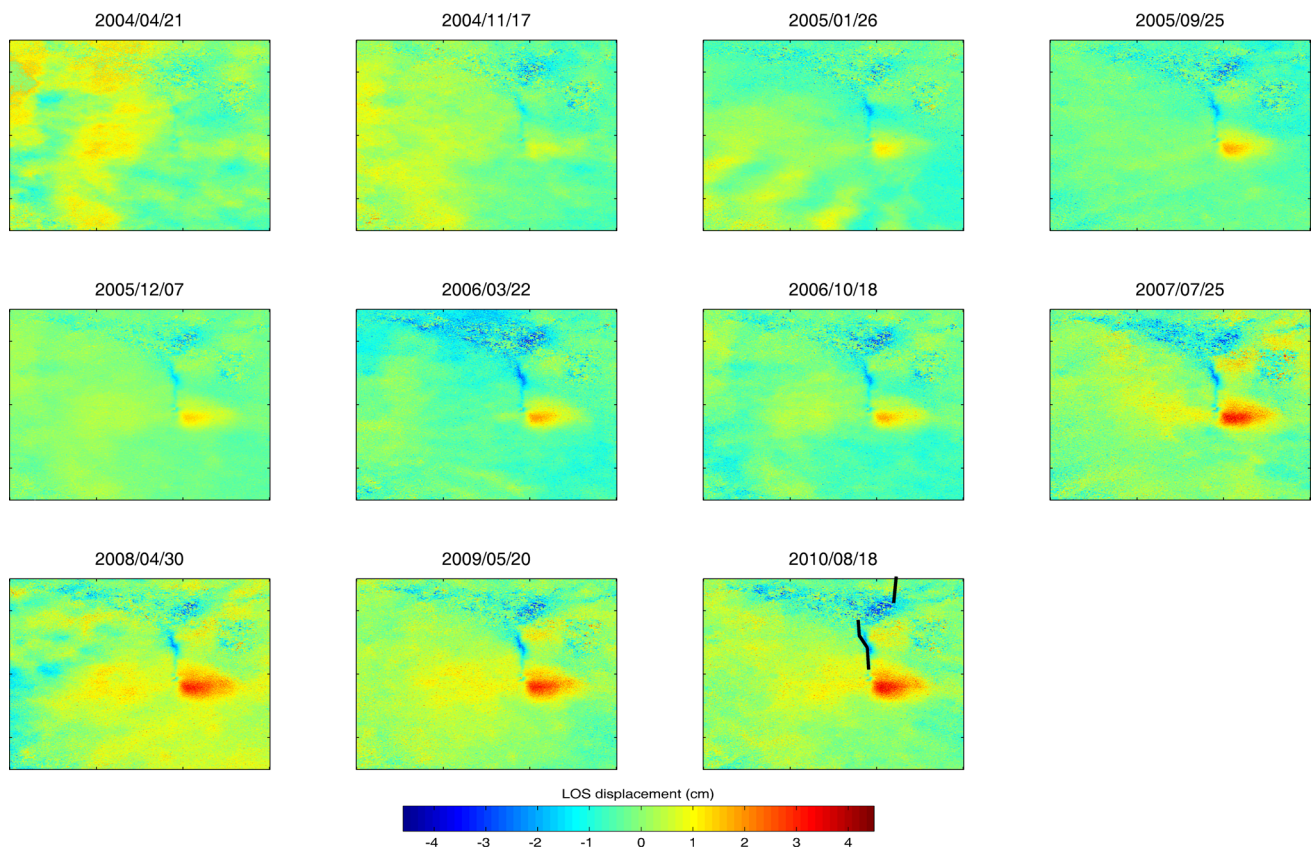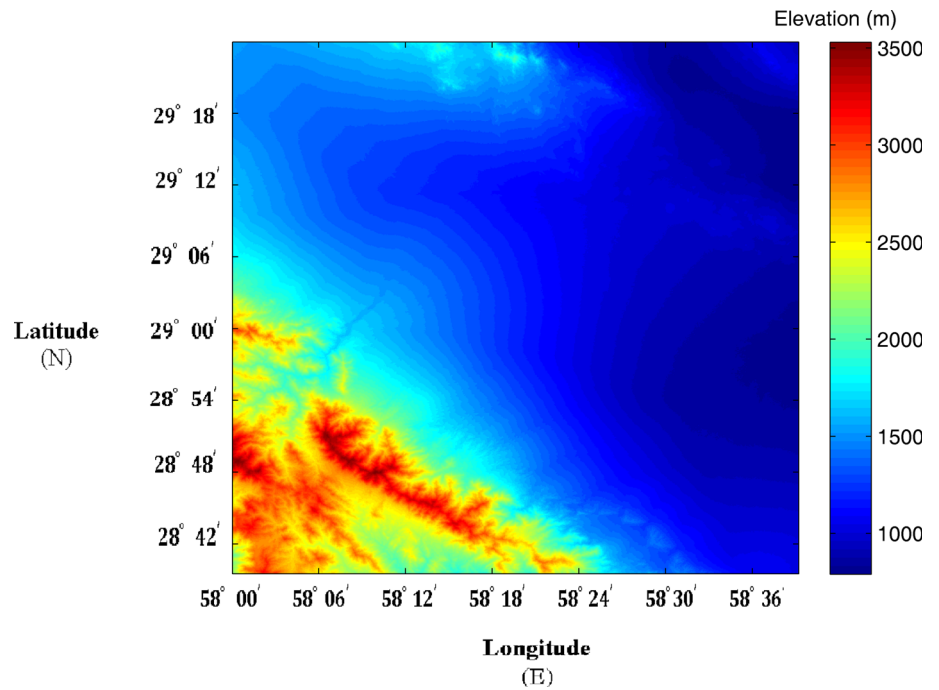
Fig. 3 Postseismic time series following Bam, Iran earthquake in near-fault field. *Black Lines* in *bottom image* marks location of Bam faults

Fig. 4 Postseismic displacement field following the 2003 Bam earthquake and fault location. Interfrogram is for date from 2004/02/11 to 2010/08/18. *Black line with number (1)* indicated previously mapped Bam fault and *black line with number (2)* marks earthquake unknown blind strike slip fault. (A) is a lobe of positive line of sight motion (towards the satellite locations) and (B) is a negative LOS motion over the Bam fault zone
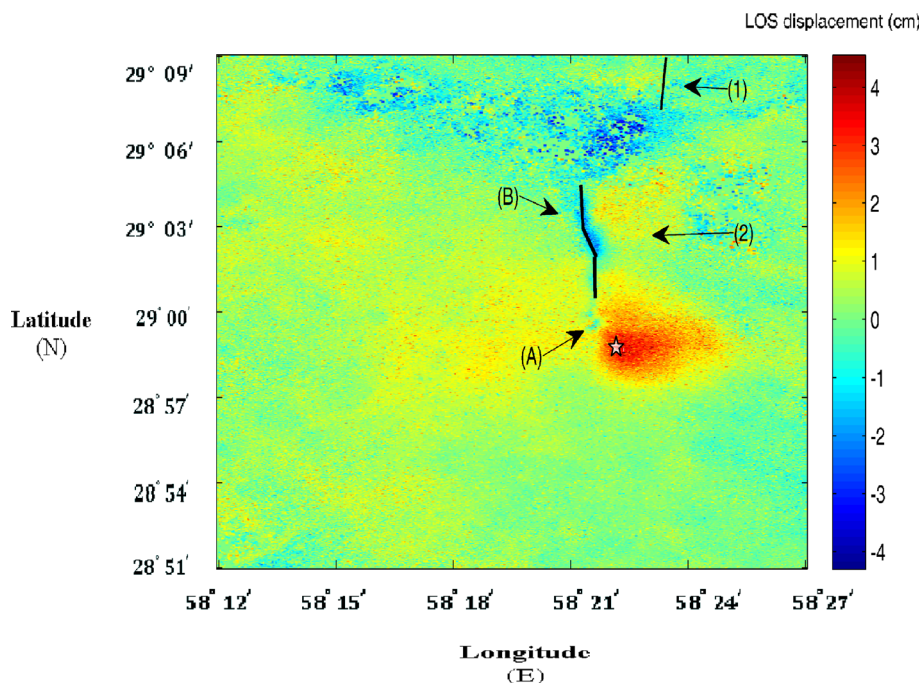


Fig. 5 Standard deviation of Bam, Iran earthquake
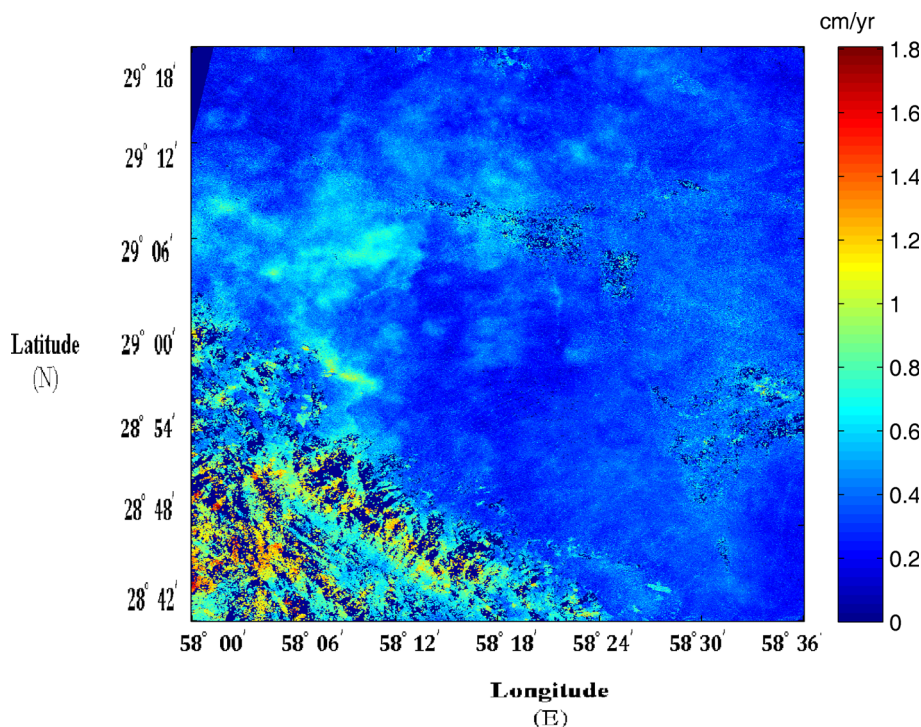
To gain a first order idea of the rate of decay of surface displacement, range change decay curve has been demonstrated for point with (55°22′48″, 28°58′48″) coordinate shown with start in Fig. 4. To improve the precise, range change decay curves have been shown for three points around this point. It is shown in Fig. 6 that exponential function can be fitted for post-seismic processes. The function has the form

$$A + B \times (1 - e^{-t/\tau}),$$

where A, B and τ are constants (A = −20 mm, B = 38 mm, τ = 2.5 years) and t is time in years since

Fig. 6 Range change decay curves for point with (55°22′48″, 28°58′48″) coordinat. The best fitted model to the deformation time series is function $A + B \times (1 - e^{-t/\tau})$ for uplift region
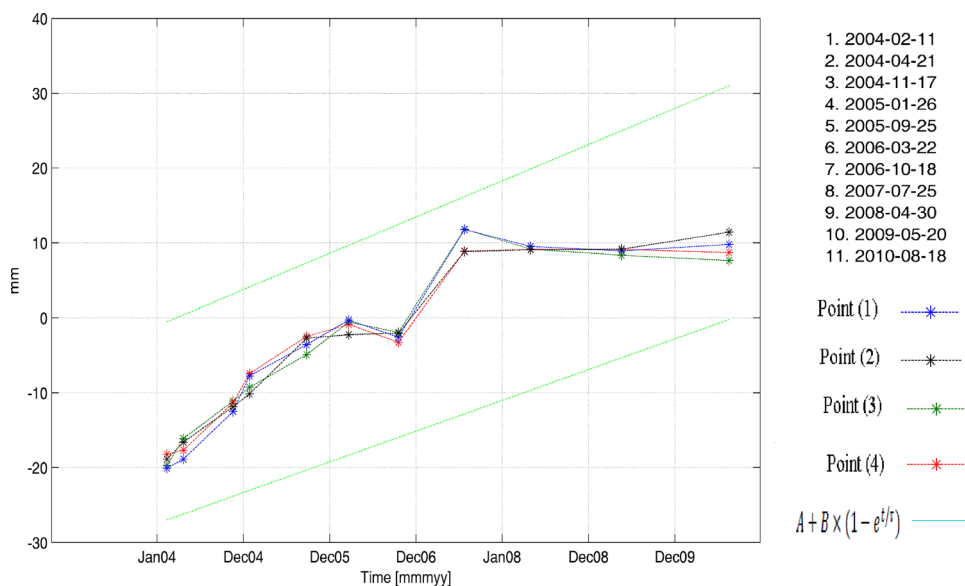
Table 2 Source parameters of Bam earthquake which was obtained by an inversion procedure (Funning et al. 2005)

Fault	Lat (°)	Long (°)	Depth (km)	Strike (°)	Dip (°)	Rake (°)	Slip (m)	Length (km)	Width (km)
1	28.988	58.406	6.7	180.0	63.9	149.5	2.04	14.8	1.4
2	29.038	58.357	5.5	354.6	85.5	−177.8	2.14	12.0	8.6

the earthquake (e.g., Peltzer et al. 1998; Perfettini and Avouac 2004; Ryder et al. 2007; Li et al. 2009). In Fig. 6 displacement velocity decreases with time and approaching to the inter-seismic behavior. The relaxation time is 2.5 years.

Modeling

Four different modeling approaches were used to try and understand the observed variations in surface displacement. Post-seismic four models: poroelastic rebounds, afterslip, viscoelastic stress relaxation and dilatancy recovery are treated separately for modeling purposes, though it is acknowledged that more than one mechanism may occur at any one time (Ryder et al. 2007). Bam faults geometry which is extracted from inversion of co-seismic deformation is shown in Table 2 (Funning et al. 2005).

Poroelastic Rebound

Poroelastic rebound model assumes that post-seismic deformation are caused by the diffusion of pore pressure change due to the flow of pore fluid. On the basis of theoretical arguments, pore fluid diffusion should occur at intermediate wavelengths from near field to about 2.5 fault lengths from the fault (Piombo et al 2005). Radar

interferometry is highly sensitive to the vertical component of the deformation field and is therefore well suited for the detection of poroelastic rebound (e.g., Peltzer et al. 1998; Barbot et al. 2008). The transient behavior can be approximated by a temporary increase in the Poisson's ration, representing the initial change in pore-fluid pressure which decays back to the pre-earthquake equilibrium value. There is a gradual change of Poisson's ration in the crustal rocks from the undrained (co-seismic) conditions immediately after the earthquake to lower, drained (post-seismic) values (Peltzer et al. 1998).

Hence the surface motion resulting from pore fluid flow can be estimated from the difference between the co-seismic displacement fields calculated using different Poisson's ration elastic models. Here, a homogenous half space model has been used to explain observed post-seismic deformation.

The difference in Poisson's ration is typically 0.03 (Peltzer et al. 1996). Surface displacements have been computed by choosing values of the undrained Poisson's ration $v_d = 0.25$ and the drained Poisson's ration $v_u = 0.22$. With the aim of producing a projection from 3D displacement vectors $\vec{d} = (d_v, d_n, d_e)$ on to line-of-sight direction $\vec{d}$ the following equation was generated.

$$d = \delta_r + \vec{d}_v \times \cos\theta_{inc} - \sin\theta_{inc}\left[\vec{d}_n \times \sin H - \vec{d}_e \times \cos H\right]$$

(4)

where θ_{inc} is the incidence angle, H is the heading angle (positive clockwise from the north), $\vec{d} = (d_v, d_n, d_e)$ indicates deformations in vertical, north and east directions and δ_r is measurements' errors based on atmospheric noise, DEM errors etc (Erten et al. 2007).

Figure 7a demonstrate the obtained results of the poroelastic rebound model, projected onto the LOS direction and Fig. 7b demonstrate the correlation between the

poroelastic rebound model and the InSAR derived displacement field, respectively.

Afterslip

According to the afterslip hypothesis, crust deformation after an earthquake originates as a slow slip on the original fault surface or along the extended surface of the original

Fig. 7 Prediction of the poroelastic rebound model after Bam, Iran earthquake and projected in the LOS direction. **a** Poroelastic rebound model, **b** correlation between the poroelastic rebound model and the InSAR derived displacement field
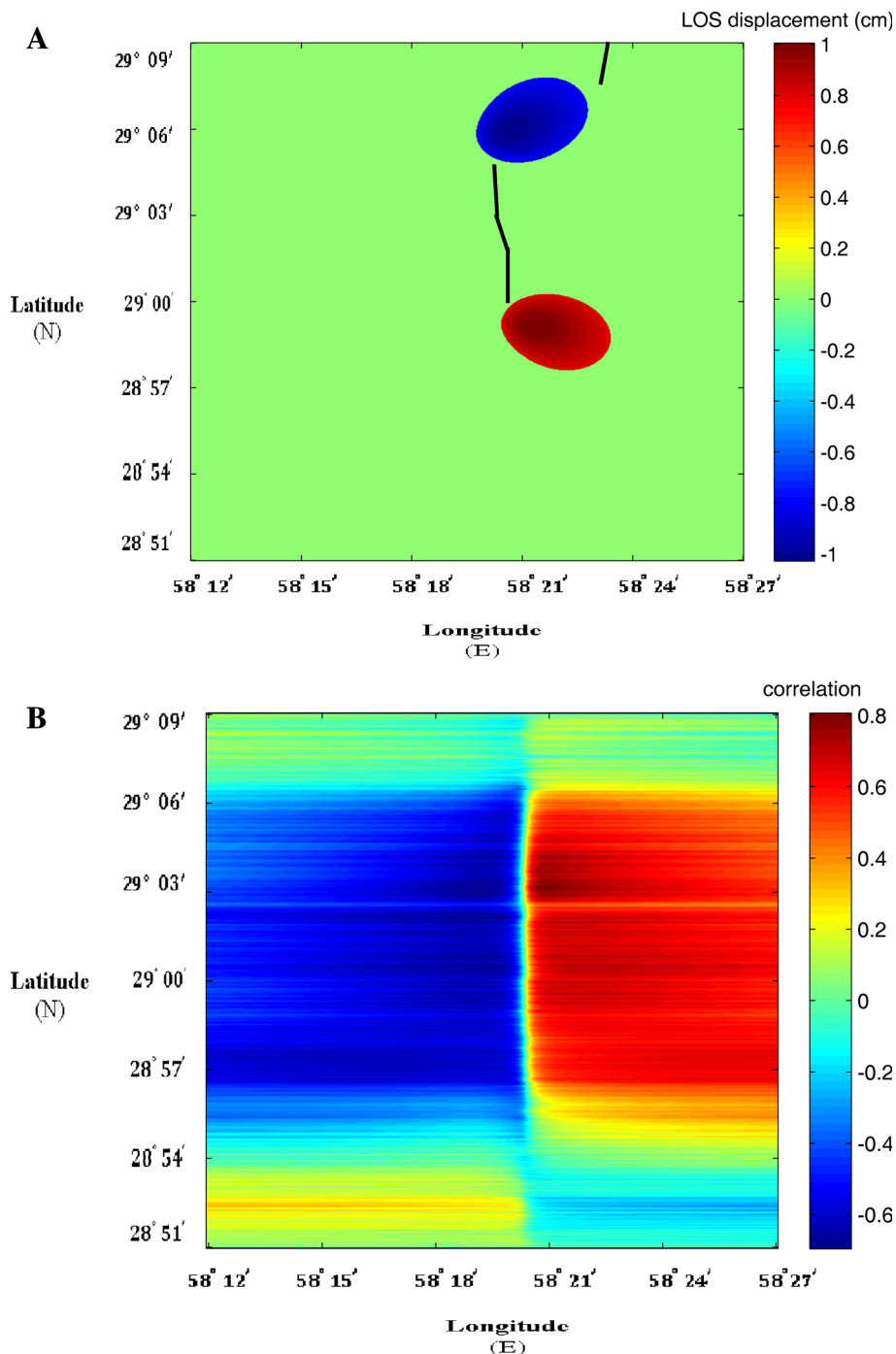
Fig. 8 Inversion of postseismic interfrograms for afterslip model. **a** Afterslip model, **b** correlation between the afterslip model and the InSAR derived displacement field
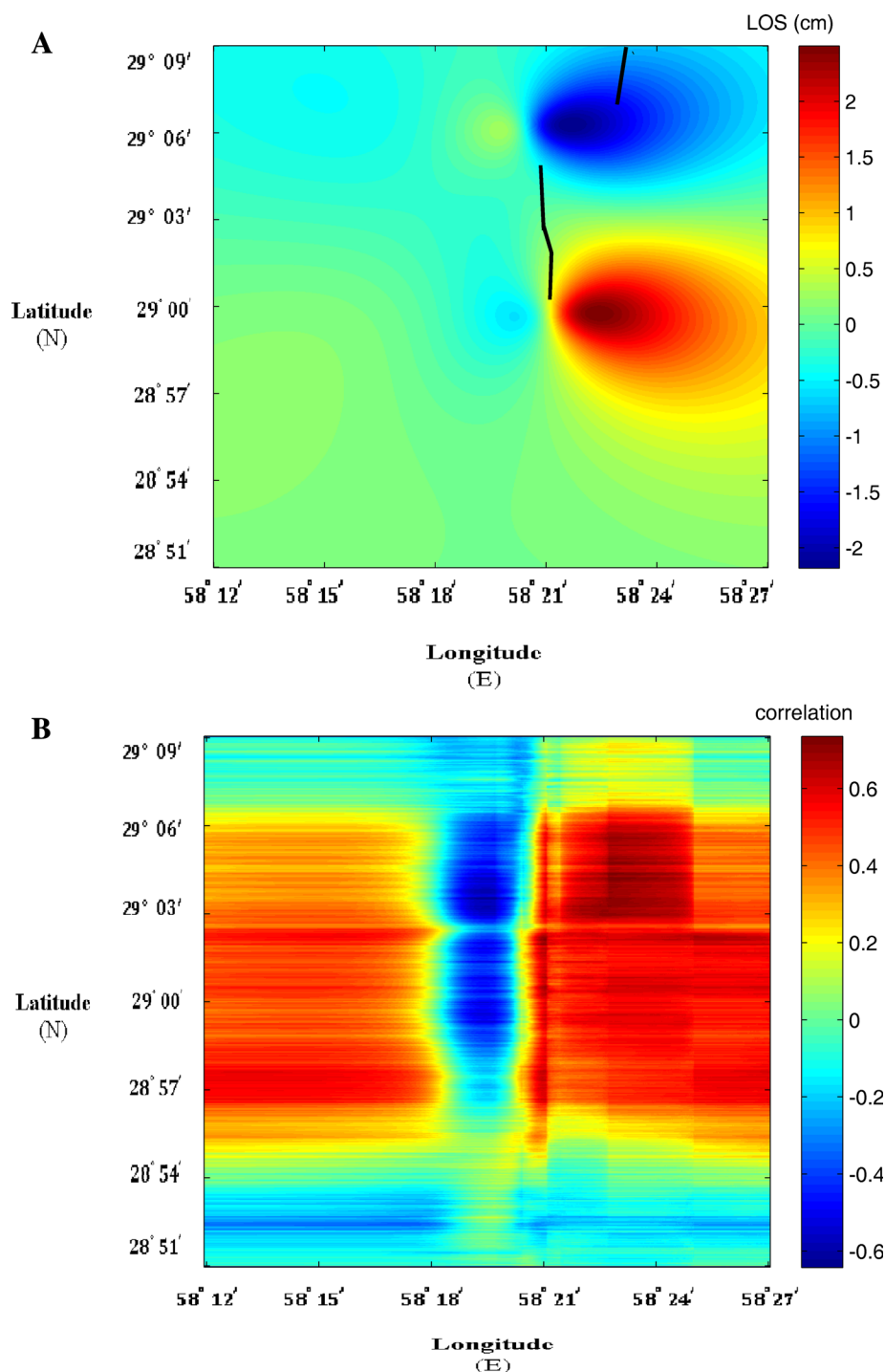

fault. Afterslip is based on rate and state variable friction laws (Marone et al. 1991). Recent studies show that afterslip can be the plausible mechanism responsible for post-seismic transients, at least in some locations (Barbot and Fialko 2010; Ryder et al. 2007), but it may also occur in combination with other mechanisms (Wang et al. 2009). For this part of modeling it has been assumed that afterslip on the fault and its extension at depth is responsible for post-seismic motion. In this paper slip model for the Bam

earthquake was obtained from the inversion of SAR line-of-sight data, using an elastic half-space solution (Okada 1985). For this purpose tow planar faults of co-seismic model have been used. The observed surface displacements are linear with respect to the afterslip by

$$u = Gs \qquad (5)$$

where G is Green's function matrix, and s represent the data, that is line-of-sight displacement and the model
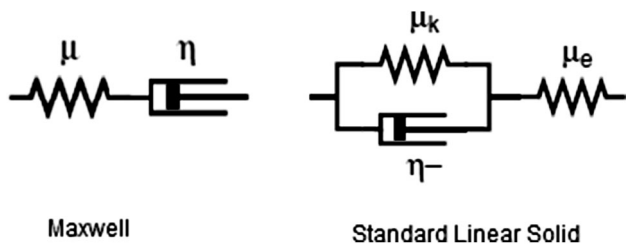
Fig. 9 Schematic illustration of simple mechanical analogues for Maxwell and standard linear solid rheologies (Ryder et al. 2007)

Table 3 Horizontal layer structure of Bam fault

Depth (km)	v_p (km s^{-1})	v_s (km s^{-1})	ρ (10^3 kg m^{-3})	η (pa s)
5	5.577	3.217	2.6	
10	5.830	3.464	2.6	
15	5.929	3.512	2.6	
20	6.000	3.509	2.6	10^{19}
25	6.032	3.500	2.6	10^{19}
30	6.045	3.500	2.6	10^{19}

solution, that is post-seismic slip, respectively. Analytical expression has been developed for Green's function in elastic half-space (Okada 1985). Because relation between displacement and slip is linear, Eq. (5) is usually solved by the least-squares inversion method.

$$\hat{S} = \begin{bmatrix} G^T & C_u^{-1}G \end{bmatrix}^{-1} G^T \quad C_u^{-1}u \tag{6}$$

And precision of slip obtain by:

$$\sigma_{\hat{s}} = \begin{bmatrix} G^T & C_u^{-1}G \end{bmatrix}^{-1} \tag{7}$$

The estimated post-seismic slip value is s = 20.45 ± 0.38 cm.

Figure 8a, b demonstrate the obtained results of the afterslip modeling and the correlation between the afterslip

model and the InSAR derived displacement field, respectively. The afterslip model has the predominant contribution to the post-seismic displacement field.

Surface deformation showing Most of the post-seismic displacement field can be explained in terms of fault slip.
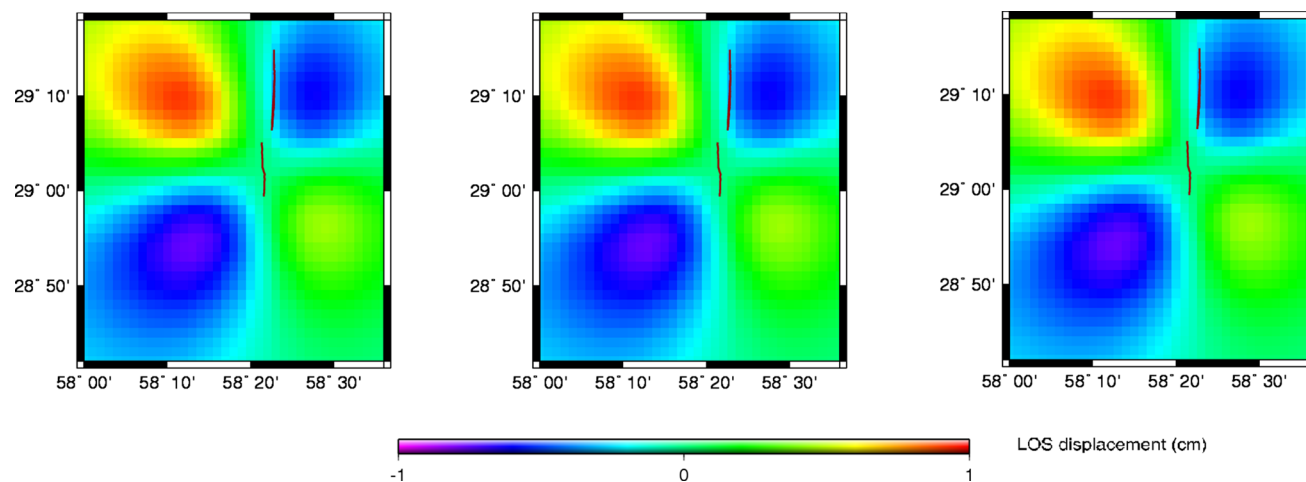
Viscoelastic Relaxation

A possibility of a viscoelastic response has been investigated by using a rheological model of China proposed by Wang et al. (2006). The model consists of a multilayered viscoelastic half-space. Compared with the afterslip and poroelastic rebound mechanisms, viscoelastic relaxation normally has more significant effect on the far field or on the long term deformation (Pollitz et al. 2000; Wang et al. 2009). The far field or long-term data normally have low displacement values. In this study two linear viscoelastic rheologies have been considered: Maxwell and standard linear solid. This viscoelastic models described in Fig. 9, where μ_e is unrelaxed shear modulus, η is viscosity and $\frac{\mu_k\mu_e}{\mu_k\mu_e}$ is relaxed shear modulus.

The complex shear modulus for SLS rheology is then given by:

$$\mu(i\omega) = \mu_e \frac{(1-\beta)\mu_e + \beta i\omega\eta}{\mu_e + \beta i\omega\eta} \tag{8}$$

where ω is frequency and $\beta = \frac{\mu_e}{\mu_k+\mu_e}$ is the relaxation strength of an SLS body by value $0 < \beta < 1$, for tow special cases $\beta = 0$ and $\beta = 1$, representing perfect elasticity and Maxwell rheology, respectively. The forwarded modeling of viscoelastic relaxation has been done using the code PSGRN/PSCMP (Wang et al. 2006).

The elastic parameters of each layer are obtained from the v_P, v_S and density profiles based on Zohoorian et al. (1984) and Sadeghi et al. (2006) (Table 3). The value of viscosity for upper mantle is considered to be in the range of $\eta = 10^{18}$–10^{25} pa s. This indicates that the post-seismic

Fig. 10 Simulated LOS displacement for 3 dates after Bam earthquake of viscoelastic relaxation model
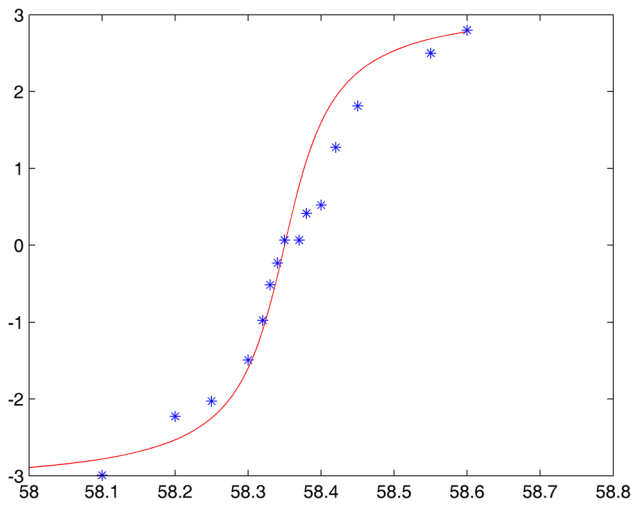
Fig. 11 Interseismic displacement after postseismic relaxation time perpendicular to the fault. *Starts* are points from InSAR displacement field and curve is the interseismic displacement obtains from model

deformation which has been observed at the surface is not sensitive to variations in rheology at depths.

We computed the entire time series of the post-seismic transient and then simulated the SAR data by computing the difference between the surface deformations corresponding to the SAR acquisition dates, projected on to satellite LOS. The resulting surface displacements for 2.5, 5 and 7 years after Bam earthquake respectively are shown in Fig. 10.

The viscoelastic modeling indicates that the calculated results have been fitted for a few observations and the effect of viscoelastic relaxation signal in post-seismic displacement is small.

Inter-seismic

In this study, post-seismic and inter-seismic deformation has been measured for ∼7 years after the 2003 Bam earthquake and post-seismic relaxation time is 2.5 years.
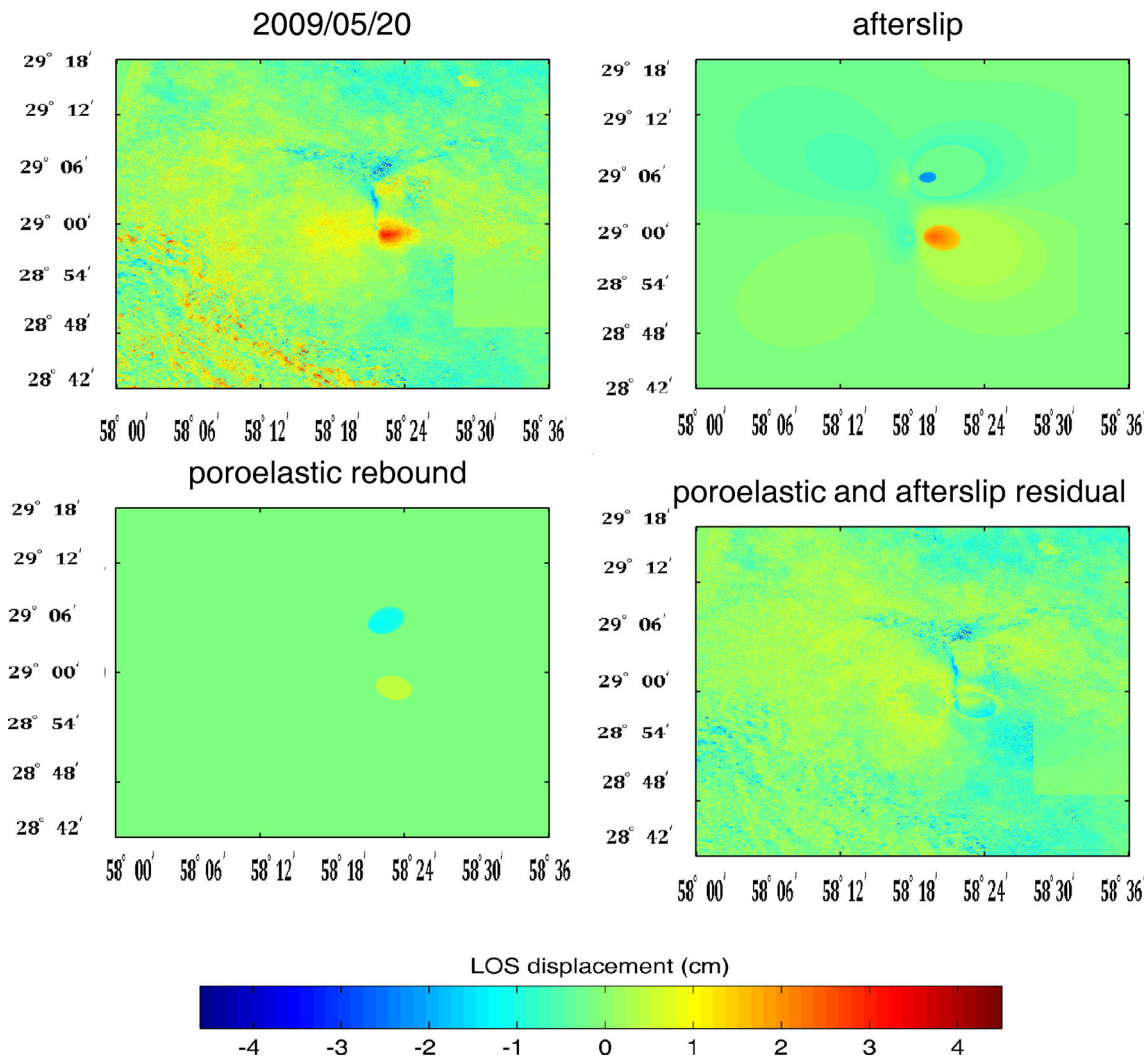
Fig. 12 The interfrogram residuals during the time interval of 2004/02/11 and 2010/08/18 has been calculated with respect to the after slip and poroelastic rebound models

So post-seismic modeling requires separation of the inter-seismic surface displacement, which can be modeled by fundamental Eq. (9) (Savage and Prescott 1978):

$$u = \frac{-s}{\pi} \times \tan^{-1}\left(\frac{x}{d}\right) \quad (9)$$

where x is the distance perpendicular to fault, s is slip rate and d is locking depth. We estimate the inter-seismic slip using the inversion of SAR line-of-sight data after relaxation time. The estimated inter-seismic slip value after relaxation time to 2010/08/18 is 6.35 ± 0.05 mm. In Fig. 11 starts are points from InSAR displacement field after decay time to 2010/08/18 and curve is the inter-seismic displacement obtains from model. The root mean square between model and data is 0.98 mm.

Discussion

In this paper the interfrogram residuals during the time interval of 2004/02/11 and 2010/08/18 has been calculated with respect to the after slip and poroelastic rebound models.

Result is shown in Fig. 12. The relaxation time for Bam fault is 2.5 years and poroelastic rebound occurs in a short time period of months, then negative LOS motion over the Bam fault zone cannot be detected with poroelastic rebound. The negative LOS motion over the Bam fault zone correspond with the recovery of dilatancy and the rest of the signal is related to viscoelastic relaxation.

Fielding removed any long-wavelength deformation signal but we obtained displacement field that has longer magnitude due to their displacement. In this paper post-seismic deformation due to poroelastic rebound, viscoelastic relaxation, afterslip and dilatancy recovery have been investigated (Fielding et al. 2009).

Conclusions

The results of Bam post-seismic displacement field illustrate that the maximum amount of positive line of sight motion (towards the satellite locations) and negative LOS motion over the Bam fault zone, during 2004–2010 after the earthquake are 4.5 ± 0.5 and -4.3 ± 0.5 cm, respectively. Exponential model can be fitted for post-seismic processes. In this model, displacement rate decreases with time, which represents achieve the inter-seismic stage in the earthquake cycle (earthquake cycle: inter-seismic, co-seismic, post-seismic).

The post-seismic deformation can be simulated by integration of four models. Bam post-seismic displacement field, as observed from all interferograms is most compatible with afterslip model. Post-seismic modeling shows that a negative LOS motion over the Bam fault zone is most due to dilatancy recovery. The results of modeling the post-seismic motion indicates that line-of-sight data can be explained with the poroelastic rebound model and effect of viscoelastic relaxation in post-seismic displacement is small. Post-seismic modeling has been separated of the inter-seismic surface displacement. The estimated inter-seismic slip value after relaxation time to 2010/08/18 is 6.35 ± 0.05 mm.

References

Amighpey, M., Voosoghi, B., & Motagh, M. (2014). Deformation and fault parameters of the 2005 Qeshm earthquake in Iran revisited: A Bayesian simulated annealing approach applied to the inversion of space geodetic data. *International Journal of Applied Earth Observation and Geoinformation, 26,* 184–192.

Barbot, S., & Fialko, Y. (2010). A unified continuum representation of post-seismic relaxation mechanisms: Semi-analytic models of afterslip, proelastic rebound and viscoelastic flow. *Geophysical Journal International, 182,* 1124–1140.

Barbot, S., Hamiel, Y., & Fialko, Y. (2008). Space geodetic investigation of the coseismic and postseismic deformation due to the 2003 M_w 7.2 Altai earthquake: Implications for the local lithospheric rheology. *Journal of Geophysical Research, 113,* B03403.

Erten, E., Reigber, A., & Hellwich, O. (2007). Generation of three-dimensional deformation map at low resolution using a combination of spectral diversity via least aquare approach. In *Envisat Symposiom, Montreux, Switzerland 23–27,* (ESA SP-636, July 2007).

Ferretti, A., Prati, C., & Rocca, F. (2000). Nonlinear subsidence rate estimation using permanent scatters in differential SAR interferometry. *IEEE Transactions on Geoscience and Remote Sensing, 38*(5), 2202–2212.

Fielding, E. J., Lundgren, P. R., Bümann, R., & Funning, G. J. (2009). Shallow fault-zone dilatancy recovery after the 2003 Bam earthquake in Iran. *Letters,.* doi:10.1038/nature07817.

Funning, G. J., Parsons, B., & Wright, Tim J. (2005). Surface displacements and source parameters of the 2003 Bam (Iran) earthquake from Envisat advanced synthetic aperture radar imagery. *Jornal of Geophysical Research, 110,* B09406.

Gabriel, A. K., Goldstein, R. M., & Zebker, H. A. (1989). Mapping small elevation changes over large areas: differential radar interferometry. *Journal of Geophysical Research, 94*(B7), 9183–9191.

Hooper, A. (2006). Persistent scatterer radar interferometry for crustal deformation studies and modeling of volcanic deformation. PH.D. thesis, Standford Universit.

Hooper, A., & Bekaert, D. (2012). Recent advances in SAR interferometry time series analysis for measuring crustal deformation. *Tectonophysics, the International Journal of Integrated Solid Earth Sciences, 514–517,* 1–13.

Jackson, J., & Bouchon, M. (2006). Seismotectonic, rupture process, and earthquake-hazard aspects of 2003 December 26 Bam, Iran, earthquake. *Geophysical Journal International, 166,* 1270–1292.

Li, Z., Fielding, E. J., & Cross, P. (2009). Integration of InSAR time-series analysis and water-vapor correction for mapping postseismic motion after the 2003 Bam (Iran) earthquake. *IEEE Transactions on Geoscience and Remote Sensing, 47*(9), 3220–3230.

Marone, C., Scholz, C., & Bilham, R. (1991). On themechanics of earthquake afterslip. *Journal of Geophysics, 96*, 8441–8452.

Massonnet, D., Thatcher, W., & Vadon, H. (1996). Detection of postseismic fault-zone collapse following the Landers earthquake. *Nature, 382*(6592), 612–616.

Okada, Y. (1985). Surface deformation due to shear and tensile faults in a half space. *Bulletin of the Seismological Society of America, 75*, 1135–1154.

Peltzer, G., Rosen, P., & Rogez, F. (1996). Postseismic rebound in fault step overs caused by pore fluid flow. *Science, 273*, 1202–1204.

Peltzer, G., Rosen, P., & Rogez, F. (1998). Poroelastic rebound along the Landers 1992 earthquake surface rupture. *Journal of Geophysical Research, 103*(B12), 30131–30145.

Perfettini, H., & Avouac, J.-P. (2004). Postseismic relaxation driven by brittle creep: A possible mechanism to reconcile geodetic measurements and the decay rate of aftershocks, application to the Chi-Chi earthquake, Taiwan. *Journal Geophysical Research, 109*(B2), B02304. doi:10.1029/2003JB002488.

Piombo, A., Martinelli, G., & Dragoni, M. (2005). Post-seismic fluid flow and coulomb stress changes in a poroelastic medium. *Geophysical Journal International, 162*, 505–515.

Pollitz, F. F., Peltzer, G., & Burgmann, R. (2000). Mobility of continental mantle: Evidence from postseismic geodetic observation following the 1992 Landers earthquake. *Journal of Geophysical Research, 105*, 8035–8054.

Ryder, I., Parsons, B., Wright, T., & Funning, G. (2007). Post-seismic motion following the 1997 Manyi (Tibet) earthquake: InSAR observations and modeling. *Geophysical Journal International, 169*, 1009–1027.

Sadeghi, H., Fatemi Aghda, S. M., Suzuki, S., & Nakamura, T. (2006). 3D velocity structure of the 2003 Bam earthquake area (SE Iran): Existence of a low-Poisson's ration layer and its relation to heavy damage. *Jornal of Tectonophysics, 417*, 269–283.

Savag, J. C., & Prescott W.H. (1978). Asthenospheric readjustment and the earthquake cycle. *Journal of Geophysical Research Letters, 83*, 3369–3376

Scholz, C. H. (1974). Post-earthquake dilatancy recovery. *Geology, 2*, 551–554.

Talebian, M., & Fielding, E. (2004). The 2003 Bam (Iran) earthquake: Rupture of a blind strike-slip fault. *Geophysical Research Letters, 31*, L11611.

Wang, R., Lorenzo-Martin, F., & Roth, F. (2006). PSGRN/PSCMP- a new code for calculating co- and post-seismic deformation, geoid and gravity changes based on the viscoelastic-gravitational dislocation theory. *Computers and Geosciences, 32*, 527–541.

Wang, L., Wang, R., Lorenzo-Martin, F., & Roth, F. (2009). Afterslip and viscoelastic relaxation following the 1999 M 7.4 Izmit earthquake from GPS measurements. *Geophysical Journal International, 178*(3), 1220–1237.

Zohoorian, A., Mohajer-Ashjai, A., Kabiri, A., & Hosseinian-Ghamsari, M. (1984). Damage distribution and aftershock sequence of tow destructive earthquake in 1981 in eastern Kerman. *Journal of the Earth and Space Physics*, 10–15.